JOURNAL OF OPTOELECTRONICS AND ADVANCED MATERIALS Vol. 10, No. 11, November 2008, p. 2840 - 2853

Review Paper

Non-intrusive theromphysical property measurement by acoustic and electrostatic levitation of liquids

S. S. SADHAL*, A. Y. REDNIKOV, K. OHSAKA
Department of Aerospace & Mechanical Engineering, University of Southern California, Los Angeles, CA 90089-1453, USA

There has been a great deal of current interest in understanding the thermodynamic behaviour of liquids in the undercooled state. In industrial systems as well as in nature, liquid states are found to exist below the freezing point, especially if a pure liquid remains in a relatively undisturbed state. For undercooled liquids, the measurement of thermophysical properties such as viscosity, surface tension and thermal diffusivity present challenges because any physical interference with a probe could lead to solidification. The undercooled state is sustainable in a containerless environment that may be provided for by acoustic or electrostatic levitation. Among the methods used, the relaxation history of deformed drops as they revert back towards spherical shape is recorded and used to obtain viscosity. Similarly, the thermal relaxation of an initially heated drop is thermographically recorded and the history is used to evaluate the thermal diffusivity. Another technique involving the stimulation of thermocapillary flow on a levitated liquid sample with a laser has also been developed. Thermal measurements include additional challenges because of buoyant convection which dominates over thermocapillary flow masks the desired measurements. Therefore, drops horizontally flattened by the acoustic field are used. This procedure reduces the hydrostatic head to 0.5 mm and significantly reduces the presence of buoyant convection. In this review, some techniques involving physical and thermal manipulation of highly viscous liquids in the levitated state are discussed and the feasibility of some new methods is discussed and evaluated.

(Received September 1, 2008; accepted October 30, 2008)

Keywords: Non-contact measurement, Viscosity, Surface tension, Thermal diffusivity, Acoustic, Electrostatic, Levitation

1. Introduction

From a materials science standpoint, the fundamental interest in undercooled liquids arises from the possibilities that different crystal structures can be created through the thermodynamic path leading to homogeneous nucleation. The undercooled state refers to the situation when a liquid sustains its fluidic state even below its normal freezing point. To understand the basic thermodynamics of the undercooled state, one has to be able to carry out the measurement of the thermophysical properties in this state. Under the circumstances, conventional measuring techniques (such as with probes) are not particularly useful because by physical intrusion, bulk liquids can undergo solidification that starts taking place at one of numerous nucleation sites. For that matter, the container walls themselves can act as nucleation sites, and hamper undercooling. It is well known that levitation of a small liquid sample is an effective way to attain a large degree of undercooling. Firstly, because the small sample volume reduces the number of the potential nucleation sites and secondly, the self-contained sample is free from the possibility of nucleation at the container walls [1, 2].

In this review of previously reported results, noncontact measurement techniques for surface tension, viscosity and thermal diffusivity are discussed. It is not a comprehensive review but is limited to some developments made in the last decade, focusing particularly on high-viscosity liquids. For liquids with low to moderate viscosities, resonant-frequency methods [3, 4] have served as an effective means for viscosity and surface-tension measurement. However, for very viscous liquids, intense damping makes the resonant-frequency methods difficult to apply. For such liquids, shape relaxation of a deformed drop driven by surface tension toward a spherical shape has been effectively used [5, 6]. The relaxation phenomenon arises in natural systems as well as in industrial processes. Therefore, the physical fundamentals of drop relaxation have been of long-standing interest. The theoretical aspects of drop relaxation with small initial deformations have been studied thoroughly and various results have appeared in the literature [3, 4, 7-12]. The dynamics of relaxation is affected considerably by the presence of Earth's gravity, and this has hampered some measurements where surface tension-driven relaxation is small enough to be comparable to gravitational deformation. As a means to mitigate gravitational effects, viscous liquid drops were acoustically levitated and rotated to cause elongation [5]. The relaxation was initiated by turning off the acoustic torque and the recorded history of the process allowed the inference of the viscous properties.

The other approach to minimizing gravitational effects is to utilize microgravity environments. Short duration microgravity environments up to 30 seconds can be created by the drop tube/tower facilities and the parabolic flight of aircrafts. Long-duration microgravity environments can be created onboard spacecraft orbiting around Earth [13]. While long-duration microgravity environments have been

generally preferable, the studies on the shape relaxation of acoustically levitated drops [5] showed that some drops completed the relaxation in short times (of the order of seconds). In light of this observation, an experiment in which an initially levitated drop was suddenly released and allowed to fall freely for a short distance of several millimetres [6], was performed. The history of the shape relaxation during the free fall was characterized in terms of the change in the aspect ratio. The results were then compared with a simple linear relaxation model. This is a unique experiment employing a compact and inexpensive tabletop apparatus in contrast to the experiments utilizing the conventional microgravity facilities that are structurally extensive and require large resources.

The levitation approach has been used to measure other thermophysical properties of undercooled liquid drops such as density [1, 14], surface tension [15], and heat capacity [1]. More recently, Ohsaka and coworkers [5, 6] presented techniques for thermal diffusivity measurement with the use of levitated liquids. Two separate methods have been employed. Both used laser-heating as a thermal stimulus on a levitated liquid sample, and employed an acoustic field for levitation and an infrared (IR) camera as a thermal diagnostic device. Glycerin drops, whose thermal diffusivity coefficient is well known, was used as a model liquid to demonstrate the feasibility of these techniques. The first one [16] was based on pure diffusion thermal transport in the drop that was rotated about a vertical axis so that the spot-heating was effectively axisymmetric in a time-average sense on the edge of the drop. The heating was turned off after some time and the thermal relaxation towards isothermal conditions was recorded thermographically and used to calculate the thermal diffusivity. With the second approach [17], laser-heating was applied on a spot on the edge so that non-axisymmetric heating took place. Additionally, the heating intensity was sufficient to create thermocapillary flow. The challenge with this technique is to suppress buoyancy-driven flow. This was done by horizontally flattening the levitated drop with an intense acoustic field to a thickness of 0.5 mm, thereby significantly reducing the gravitational potential within the drop. The thermocapillary flow field, along with the thermographic temperature images, was recorded. At the same time, a theoretical model based on lubrication theory for these quantities was developed and used to solve the inverse problem of calculating the thermal diffusivity. This also entailed some calculations for thermal transport with acoustic streaming [18] which is inherently different from the conventional boundary-layer convection. This method did not significantly improve the accuracy over the thermal relaxation approach, and therefore will not be discussed in much detail.

2. Surface tension and viscosity measurement of molten metals

Rhim, Ohsaka, Paradis & Spjut [2] have carried out viscosity and surface tension measurements of molten tin and zirconium by electrostatically levitating drops of these materials and applying weakly damped oscillations. The measured oscillation frequency was correlated to the surface tension and the damping constant to the viscosity. The basic theory is described next.

2.1 Theory

For a liquid drop undergoing small-amplitude axisymmetric oscillations, the drop shape in terms of the radial distance $r(\theta, t)$ in the usual spherical coordinates is described by

$$r(\theta,t) = r_0 + \sum_{n=2}^{\infty} r_n \cos(\omega_n t) P_n(\cos\theta) \exp(-t/\tau_n), \quad (1)$$

where r_0 is the spherical radius of the drop, $P_n(\cos\theta)$ represents Legendre polynomials, and r_n is the oscillation amplitude of the nth mode. The set of damping constants τ_n is related to the sample kinematic viscosity $\nu = \eta/\rho$ as follows:

$$\frac{1}{\tau_n} = n(n-1)(2n+1)\frac{\upsilon}{r_0^2}, \quad (2)$$

and the frequency ω_n is related to the surface tension σ by

$$\omega_n^2 = (n-1)(n+2)\frac{\sigma}{\rho r_0^3} \quad (3)$$

The mode n=2 is the dominant mode of oscillation and the corresponding parameters are

$$\frac{1}{\tau_2} = \frac{5\upsilon}{r_0^2} \quad \text{and} \quad \omega_2^2 = \frac{8\sigma}{\rho r_0^3} \quad (4)$$

The relationship between frequency and surface tension is in the absence of any charge. However, with electrostatic levitation, when charge is present, the Rayleigh correction [19] is required, resulting in the following expression for the for the oscillation frequency in the mode $P_2(\cos\theta)$.

$$\omega_{2c}^2 = \frac{8\sigma}{\rho r_0^3}\left(1 - \frac{Q_s^2}{64\pi^2 r_0^3 \sigma \varepsilon_0}\right), \quad (5)$$

The surface tension then takes the form

$$\sigma = \frac{r_0^3 \rho}{8}\left(\omega_{2c}^2 + \frac{Q_s^2}{8\pi^2 r_0^6 \rho \varepsilon_0}\right), \quad (6)$$

For charge measurement purposes, the simple force balance

$$mg = \frac{Q_s V}{L}, \quad (7)$$

was used. Here V/L represents the electric field due to two parallel plates a distance L apart with a potential difference V. These results are based on the linear theory of drop oscillations. The analysis of Feng & Beard [20] on nonlinear effects has led to a correction which, for the mode $n = 2$ is

$$\omega_{2c}^2 + = \omega_{2c}^2 \left[1 - \frac{(2.43.31\sigma^2 - 63.14q^2\sigma + 1.54q^4)e^2}{176\sigma^3 - 120q^2\sigma^2 + 27q^4\sigma - 2q^6} \right], \quad (8)$$

where q and e are defined by

$$q^2 = \frac{Q_s^2}{16\pi r_0^2 \varepsilon_0} \qquad \text{and} \qquad e^2 = E^2 r_0 \varepsilon_0 \quad (9)$$

with E being the applied electric field.

2.2 Experimental procedure and data analysis

The technique involves a high-temperature electrostatic levitator (HTESL) which consists of two horizontal electrodes about 12 mm apart, as shown in Fig. 1. The details can be seen in [2]. This system is capable of levitating a 1-3 mm diameter sample between a pair of parallel-disk electrodes placed 12 mm apart. The oscillations were excited by an AC voltage amplifier inserted between the bottom electrode and the ground (see Fig. 1). Backlighting along with shadowgraphy and photodetection was used as a method of visualization of the oscillation profile. A sinusoidal pulse of a given frequency and amplitude was input at the lower electrode, and the ensuing signal was taken to have the form

$$y = Ae^{-t/\tau} \sin(2\pi ft + \varphi), \quad (10)$$

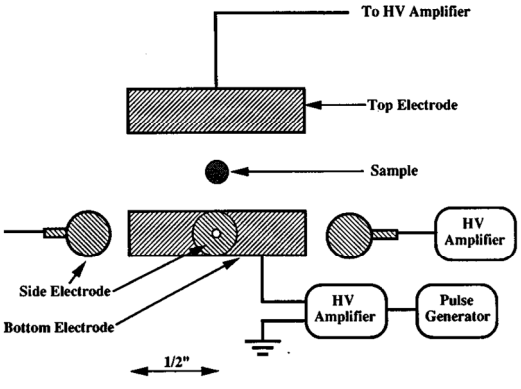

Fig. 1. Schematic of the electrode arrangement for induction of drop oscillations [2].

for which a least-squares fit was used to determine the frequency f and the decay constant τ. These parameters were then used to obtain the surface tension and viscosity using equations (5-9). The results for the surface tension of tin as a function of temperature are exhibited graphically in Fig. 2, and correlated by the formula

$$\sigma(T) = [541.3 - 0.09(T - 505)] \times 10^{-3}\ \text{Nm}^{-1}, \quad 493\text{K} \le T \le 723\text{K} \quad (11)$$

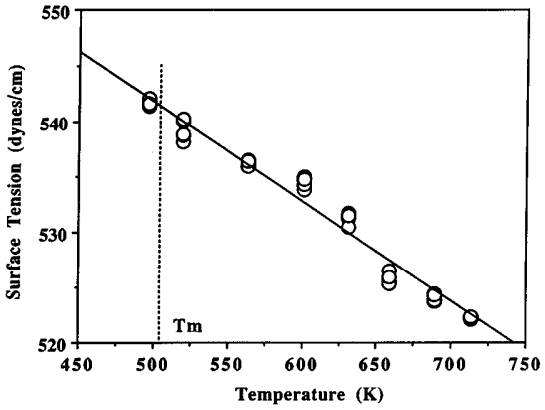

Fig. 2. Surface tension vs. temperature for of a tin sample. The vertical line at 505 K indicates the normal melting point [2].

The surface tension values from these noncontact experiments are somewhat lower than what was found in prior investigations. This discrepancy is attributed to surface contamination. From the value of the decay constant τ, Equation (4) was used to obtain the viscosity $\eta = \nu\rho$. A plot of the experimental results is given in Fig. 3.

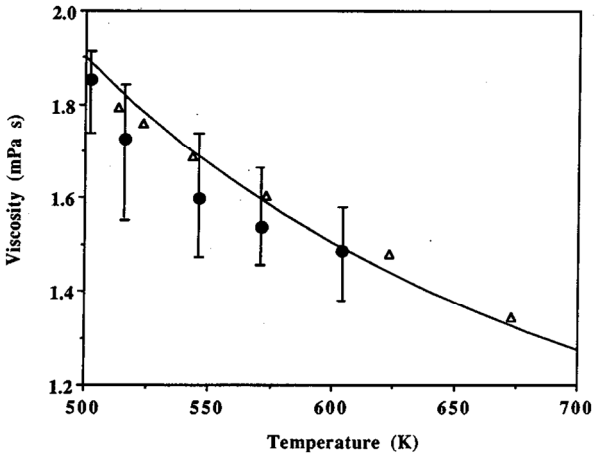

Fig. 3. Viscosity vs. temperature for the tin sample. The error bars show the spread of the data when repeated five times at each temperature. The closed circles indicate the average of the five data points. The solid curve is the fitted data (open triangles) from reference [21]. *Reproduced from* [2].

Additional experiments were carried out with zirconium for which the correlations are

$$\sigma(T) = 1.543 - 0.00037(T - 2128) \quad \text{Nm}^{-1} \quad (12)$$

and

$$\eta = 4.86 - 5.3\times10^{-3}(T - 2128) \quad \text{mPa s} \qquad (13)$$

both in the range 1850-2200 K. For this experiment, deep undercooling of up to 300 K was achieved. These results are slightly higher than the measurements by Frohberg *et al* [22] who used an electromagnetic levitator. This discrepancy may be attributed to the magnetic field which tends to cause a slight increase in the stiffness of the drop [23].

This technique is reported to be suitable for highly reactive molten refractory materials or for highly undercooled liquids. The method is applicable to liquids in the approximate viscosity range, 1 mPa s < η <130 mPa s. Further developments for refactory metals have been discussed by Ishikawa, Paradis, Itami & Yoda [24]. In addition, there is recent work on undercooled platinum by Ishikawa, Paradis & Koike [25].

3. Viscosity determination by shape relaxation of elongated drops

For highly-viscous liquids ($\eta > 10^2$ Pa s), the technique discussed above in Section 2 is not applicable, mainly because the system is overdamped and oscillations are hardly measurable. Ohsaka, Rednikov, Sadhal & Trinh [5] used acoustic levitation to suspend a sucrose solution drop. The technique involved levitation of a liquid drop using an ultrasonic standing wave, and elongation of the drop by rotating it beyond the bifurcation point. The elongated drop was then allowed to be restored to its original shape by the surface tension driven relaxation. The time-dependent shape parameters of the relaxing drop are related to the viscosity through a relaxation model. In addition, this technique can also determine the surface tension that has a known relationship with the angular velocity at the bifurcation point.

The experimental apparatus is schematically shown in Fig. 4 and a typical sequence of the relaxation of a sucrose solution drop is shown in Fig. 5. The ultrasonic driver was operated at approximately 18 kHz and used to generate a vertical (*z*-direction) standing wave between the driver head and the reflector for levitating a drop. Two broadband audio speakers (the second one is not shown) were placed at the bottom corners of the chamber facing each other at a 90° angle. The audio speakers were operated at approximately 1.4 kHz and were used to generate lateral standing waves in the acoustic chamber. A proper torque was exerted on the drop when the relative phase of the lateral standing waves was adjusted. Two cameras were used to record the images of the levitated drop. Camera 1 recorded the side view of the drop, which typically deformed into an oblate spheroid due to the acoustic pressure. The images were used to determine the aspect ratio and the true volume of the drop. Camera 2 was set up to look down the drop through the hole made on the reflector. This camera is capable of capturing the images up to 2000 frames per second and was used to record the top view of the rotating drop at the bifurcation point and during the shape relaxation. Although the apparatus did not have the capability of controlling the sample temperature, the temperature inside of the chamber remained between 28° and 29° C throughout the measurement process. There was a size limitation on the drops being levitated and elongated beyond the bifurcation point using this apparatus. As a result, only the measurement on the drops with 1.0 mm < R_0 < 1.5 mm could be performed. Here R_0 is the spherical equivalent radius of the drop whose volume is equal to that of the deformed drop.

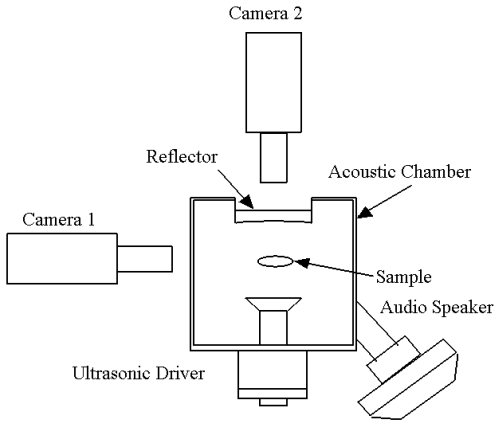

Fig. 4. Schematic diagram of the apparatus [5]

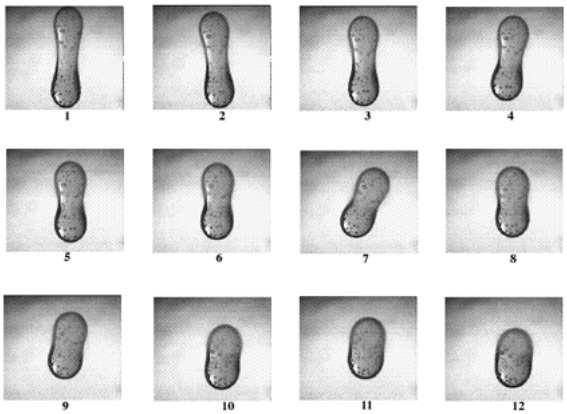

Fig. 5. A sequence of the shape relaxation of the initially elongated drop with $\eta = 1.4 \times 10^{-3}$ Poise *at* 28° C [5].

Samples of sucrose (sugar) solution were selected as a model liquid, mainly because their viscosities could be easily varied over many orders of magnitude at room temperature by adjusting the water content. A small amount of the solution was attached to the tip of a needle and inserted into the levitation chamber. The solution was gradually detached from the needle by gravity and acoustic radiation pressure, and shaped into a drop. Once the drop was completely detached, it was formed into an oblate spheroid due to the force balance among the surface tension, gravity and the acoustic forces. The levitation parameters were then adjusted so that the drop became stationary. The image of

the stationary drop was digitally recorded for the volume determination. The audio speakers were then turned on to exert a torque on the drop. The drop started rotating and expanded laterally as the rotation rate increased. The high-speed camera continuously monitored the rotation of the drop and recorded the moment of bifurcation for the angular velocity determination. After bifurcation, the drop evolved into a two-lobed shape and continued to elongate until the torque was suddenly removed by turning off the audio speakers just before fission would occur. The elongated drop immediately started decelerating due to air drag and eventually stopped rotating. In order to shorten the deceleration stage, a counter torque was briefly applied by reversing the phase difference of the lateral standing waves before turning off the speakers in some cases.

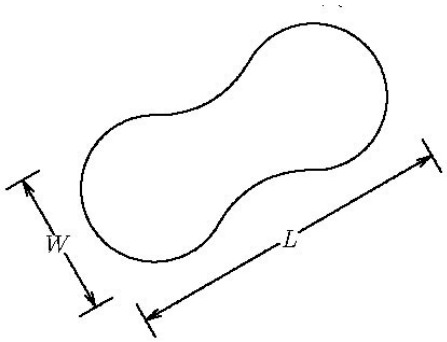

Fig. 6. A Schematic depicting the measured dimensions in the relaxation experimen. [5].

The shape evolution of the drop during the deceleration and subsequent non-rotating stages was recorded for the relaxation rate determination. The images taken initially and during the relaxation were analyzed using commercially available software to determine the volume of the drop and the variation of the dimensions of the elongated drop during the relaxation. Two representative dimensions of the elongated drop, the length, L, and the maximum width, W, as a function of the elapsed time were measured. This is shown schematically in Fig. 6. These parameters were related to the viscosity by a relaxation model of Mo, Zhou & Yu [26] that has been successfully used for the determination of the interfacial tension between two immiscible polymer melts. The model relates the shape evolution during relaxation to the physical properties of the working fluids. In their three-dimensional model, the drop shape is described by a symmetric, positive-definite, second-rank tensor $\boldsymbol{S}$ whose eigenvalues represent the square semi-axis of the ellipsoid. With some manipulation of the eignvalues of $\boldsymbol{S}$, the following relationship was obtained [5]

$$\eta = -\frac{20\sigma}{19R_0}\left[\frac{d(\ln\Psi)}{dt}\right], \tag{14}$$

where

$$\Psi = \left[\frac{L^2 - W^2}{(L^2 - W^2)_0}\right], \tag{15}$$

with L and W representing the length and the width, respectively, as mentioned above. The subscript 0 refers to some initial state. Since all the parameters in (14) and (15) that are needed to determine η are measurable quantities, the viscosity may be obtained [5].

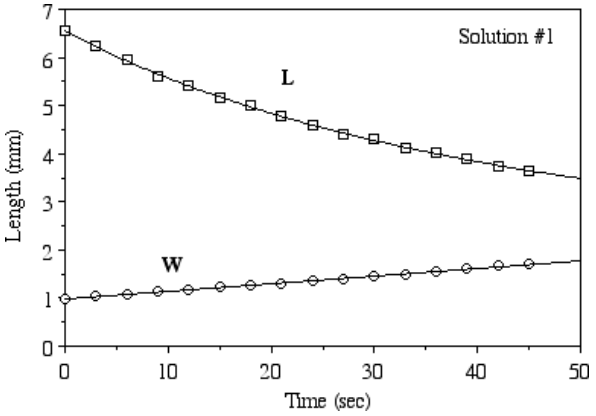

Fig. 7. Measured values of L and W as a function of elapsed time [5].

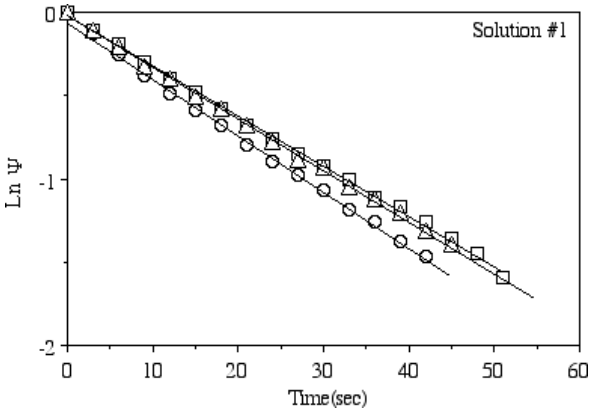

Fig. 8. Evolution of the shape parameter Ψ for $\eta = 1.2 \times 10^3$ Pa s at 28°C [5].

An interesting observation is that the data includes the early stages of relaxation when the drop is actually two-lobed. In spite of this deviation from the ellipsoidal shape, the linear fit works unexpectedly well. For comparison, the viscosity of the solutions was also determined by a falling ball technique that was commonly used for highly viscous liquids.

As mentioned earlier, Fig. 5 shows a sequence of the shape relaxation of an elongated drop (R_0 = 1.3 mm, η = 1.2×10^3 Pa s at 28°C). The images are the top view of the drop. The small dark spots in the drop are the air bubbles of varying size. The time interval between two consecutive images is 3 seconds. The elongated drop was not completely stationary but exhibited slow rocking and

translational motion which does not significantly affect the relaxation process.

Experimental results for the sugar-solution test case have been obtained and agree quite well with measurements using the falling-ball method. The measured values of $L(t)$ and $W(t)$ show a fairly linear behaviour with time as shown in Fig. 7. The shape evolution parameter, $\ln(\Psi)$, is plotted in Fig. 8 as a function of time. A linear behaviour with a negative slope is seen, and it is quite straightforward to interpret the viscosity. An interesting observation is that the data includes the early stages of relaxation when the drop is actually two-lobed. In spite of this deviation from the ellipsoidal shape, the linear fit works unexpectedly well.

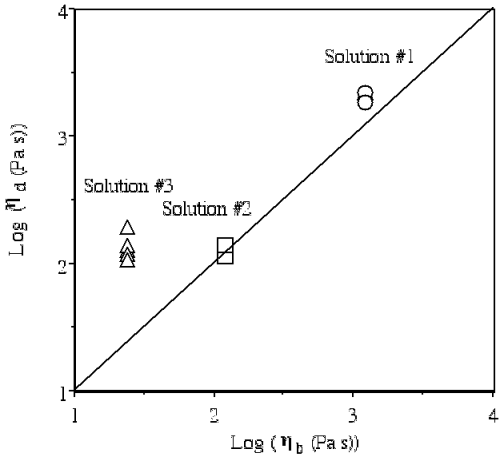

Fig. 9. Correlation between η_b determined by the falling ball technique, vs. η_d determined by the present technique on log-log scales [5].

Fig. 9 shows the viscosity, η_b determined by the falling ball technique vs. the viscosity, η_d determined by the present technique in the logarithm scale. As seen in the figure, a correlation exists for Solutions #1 and #2, but not for Solution #3. We suspect that the viscosity values for Solution #3 are strongly affected by the drop rotation that sometimes lasts more than 4 seconds. The apparatus did not have capability to vary the temperature of the drop, which prevented the performance of the measurement on actually undercooled liquids.

Because of the limited capability of the acoustic levitator, the equipment could only be used to perform the measurements on low density liquids (< 2 g/cm^3). An advantage of the present technique is its capability for determining the surface tension of the drop from the measurement of the angular velocity at the bifurcation because the normalized angular velocity has a unique value at the bifurcation point. This technique is limited to highly viscous liquids ($\eta > 10^2$ Pa s) because the rotation of the elongated drop cannot be stopped instantaneously. On the other hand, the resonant oscillation technique can only be used for low-viscosity liquids ($\eta < 10^{-1}$ Pa s). Therefore, liquids whose viscosities are in the range, 10^2 Pa s < η < 10^{-1} Pa s cannot be covered by either technique. A method suitable for this range is discussed next. While the technique has been discussed in another review [27], the results are presented here for completeness.

4. Viscosity measurement by 50 millisecond free fall

In the range 10^2 Pa s < η < 10^{-1} Pa s, a liquid drop experiences oscillations that are highly damped. It is possible to record these oscillations if the gravitational effects can be effectively neutralized. To this end, Sadhal, Rednikov & Ohsaka [6] devised a millisecond-scale free-fall table-top experiment. Sadhal, Rednikov & Ohsaka [6] employed an acoustic-electrostatic hybrid levitator to initially suspend a drop in air. With the forces due to levitation, surface tension and gravity in play, the levitated drop was deformed at equilibrium. In a levitated state, the drop assumed approximately a prolate spheroid shape in the electrostatic levitation mode and an oblate spheroid in the acoustic levitation mode. During the free fall, relaxation of the drop took place leading to a final spherical shape. Depending on the physical properties such as the volume, surface tension and viscosity, the shape relaxation proceeded in either an oscillatory or non-oscillatory manner.

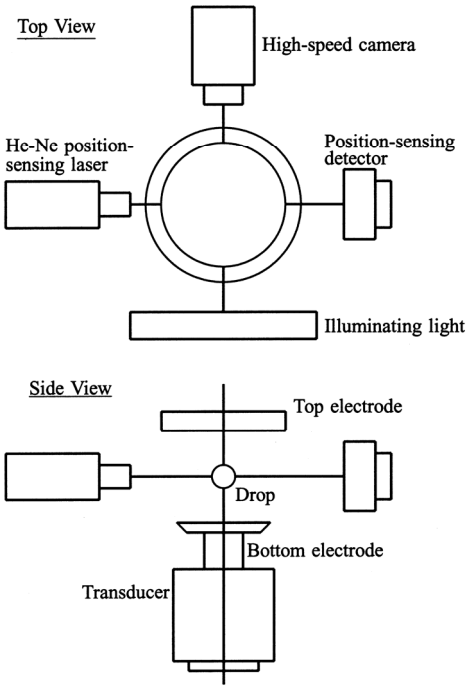

Fig. 10. A schematic description of the experimental apparatus [6].

A schematic of the table-top apparatus [6] is shown in Fig. 10. The upper and lower electrodes were 23 mm apart, and drops were typically levitated at approximately 11 mm above the lower one which was also the transducer head. The apparatus was operable in the acoustic or the electrostatic levitation modes. In the latter mode, the posi-

tion-tracking unit (laser and detector) monitored the drop position and adjusted the applied voltage 250 times per second to keep the drop at a preset position. The free fall of the drop was initiated by suddenly turning off the levitation field. Typically, the fall lasted approximately 50 milliseconds until the drop hit the bottom electrode. For about the first twenty milliseconds of the fall, the images of the drop were captured by a high-speed digital camera (operated at 1000 frame/sec). The drop was back-illuminated by white light, which created a sharply-contrasted dark image on bright background (see Fig. 11).

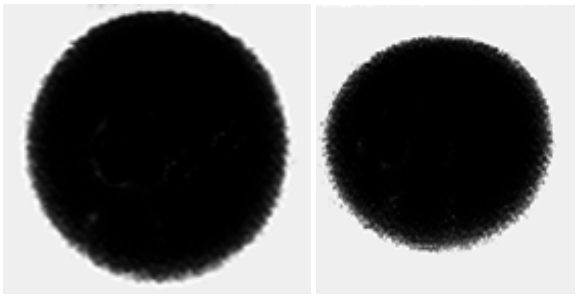

Fig. 11. Drop images: (left) an electrostatically levitated drop, (right) an acoustically levitated drop [6].

Experiments were carried out with distilled water, a water/glycerin solution and silicone oils with properties:

Test liquid	σ (mNm^{-1})	η (mPa s)
distilled water	71	1.0
water-glycerin solution	68	31
silicone-oil 1	21	10
silicone-oil 2	21	100

where σ and η are the surface tension and dynamic viscosity, respectively. A small amount of the solution (approximately 1μl) was initially suspended in the levitation field. The drop was initially in one of the following three states: (1) acoustically levitated and uncharged, (2) acoustically levitated and charged, or (3) electrostatically levitated and (necessarily) charged. The free fall was set off after the drop stabilized by turning off the levitation field. The high-speed camera captured the images that were transferred to a video recorder for analysis. Lastly, the images of a solid sphere with known radius were taken for calibration. All measurements were performed at room temperature, and the drop images recorded on videotape were transferred to a computer for the size and shape determination by commercially available software. Fig. 11 shows typical images of levitated drops in electrostatic and acoustic levitation modes. Measurements of the equatorial and polar diameters, *W*, and *H*, respectively, were carried out, and the images generally covered about 100 x 100 pixels. Since the sharpness of the edge also varied among the images, two readings for each measurement were taken. For the equatorial diameter, minimum and maximum values (W^{min} and W^{max}) were obtained by locating the edge at the respective inner and outer edges of the blur region. Similar measurements for the polar diameter (H^{min} and H^{max}) were also made, and the degree of deformation from the spherical shape was characterized by minimum and maximum aspect ratios, W^{min}/H^{max} and W^{max}/H^{min}, respectively. Additionally, the measurement of the position of the centre of mass of the falling drop allowed the determination of the acceleration of a falling drop.

4.1 Drop Deformation theory

For axisymmetric prolate/oblate drop oscillations, a linear theory was applied so that the shape of the fundamental mode ($l = 2$) could be described by the relationship [6]:

$$r(\theta,t) = a[1+\xi_2(t)P_2(\cos\theta)], \tag{16}$$

where r and θ are the spherical coordinates, a is the spherical radius of the drop, and t is the time,

$$P_2(x) = \left(\tfrac{3}{2}x^2 - \tfrac{1}{2}\right) \tag{17}$$

is the Legendre Polynomial of the order $l = 2$, and $\xi_2(t)$ is the dimensionless amplitude. Using the information that the equatorial and the polar diameters of the drop are $W = 2r(\pi/2, t)$ and $H = 2r(0, t)$, respectively, it is not difficult to show that the aspect ratio W/H is

$$\frac{W}{H} = 1 - \tfrac{3}{2}\,\xi_2(t). \tag{18}$$

For the equilibrium of a drop of mass m, carrying a total charge q, and electrostatically levitated in the middle of two parallel electrodes, the force balance is described by

$$mg = \frac{qV}{L} \tag{19}$$

where V is the applied voltage between the two electrodes, and L is the distance between the two electrodes. This equation was used to calculate the charge on the drop, all the other parameters being known. It is important to know the charge because it influences the shape-relaxation process, even though the field is turned off to release the drop into free-fall. In the study being reviewed, the drop was assumed to be a perfect conductor, while the surrounding air to be a perfect insulator. From Rayleigh's theory [19], the effect of the electrostatic force is equivalent to a reduction in the surface tension σ so that apparent value is

$$\sigma_{ap(l)} = \sigma - \frac{q^2}{(4\pi)^2(l+2)\varepsilon_0 a^3} \tag{20}$$

where l is the order of the Legendre polynomial, and ε_0 is the permittivity (SI units) in vacuum. As in equation (16) with $l = 2$, the fundamental mode of oscillation was assumed. The capillary number was defined as

$$Ca = \frac{\eta^2}{\rho\sigma_{ap(2)}a} \tag{21}$$

where ρ is the density and $\sigma_{ap(2)}$ is given by Equation (20) with $l = 2$. In the case of uncharged drops, $\sigma_{ap(2)}$ may be replaced by σ. As mentioned earlier, the dynamics of the system consists of damped oscillations. For the capillary number taking on the value $Ca_{cr} = 0.587$, the system is critically damped. For $Ca < Ca_{cr}$ the drop relaxation proceeds in an oscillatory manner (underdamped), while for $Ca > Ca_{cr}$ in a non-oscillatory manner (overdamped). The respective cases of underdamped and overdamped have been characterized by the following expressions [6] for the aspect ratio, W/H:

$$\frac{W}{H} = 1 + e^{-\delta t}(A_1 \cos\omega t + A_2 \sin\omega t), \quad (Ca < Ca_{cr}) \tag{22}$$

and

$$\frac{W}{H} = 1 + A_1 e^{-\delta_1 t} + A_2 e^{-\delta_2 t}, \qquad (Ca > Ca_{cr}). \tag{23}$$

where the amplitudes A_1 and A_2 need to be small for the linear theory to be valid. The angular frequency ω and the damping factor δ can be written in the following dimensionless forms

$$\omega^* = \left(\frac{\rho a^3}{\sigma_{ap(2)}}\right)^{1/2}\omega \qquad \text{and} \qquad \delta^* = \frac{\rho a^2}{\mu}\delta \tag{24}$$

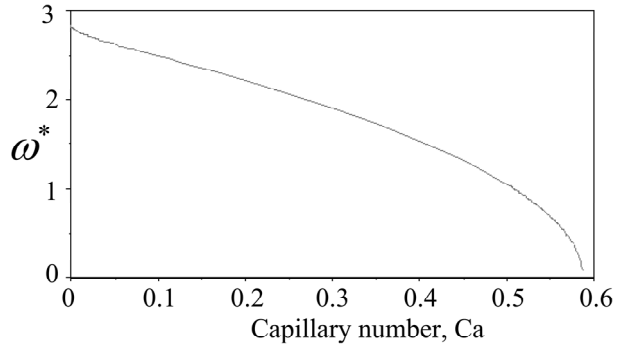

Fig. 12. Dimensionless frequency of the fundamental mode (l=2) vs. the capillary number [6].

The variation of ω^* as a function of Ca is plotted in Fig. 12, where the frequency is seen to decrease with increasing Ca and vanishes at $Ca = Ca_{cr}$. The dimensionless damping factor, δ^*, is expressed as a function of Ca in Fig. 13, where it can be seen that at $Ca = Ca_{cr}$, the value of δ^* bifurcates into two branches, δ_1^*(bottom) and δ_2^* (top). As $Ca \to \infty$, $\delta_1^* \approx (20/19)Ca^{-1}$ controls the damping rate and the second term in Equation (23) can be neglected. When Ca is close to Ca_{cr}, however, the both terms contribute to the overall relaxation. For both the cases (under- and over-damped), at $Ca = 0$, $\omega^* = \sqrt{8}$ and $\delta^* = 5$ are established [3].

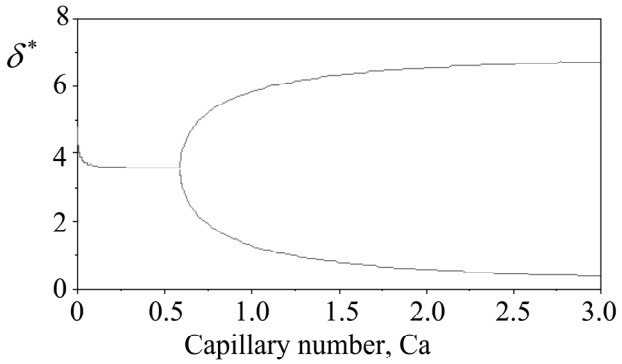

Fig. 13. Dimensionless damping rate of the fundamental mode (l=2) vs. the capillary number [6].

4.2 Experiments and Results

Several cases of test fluids were used in the experiments, and the data on the aspect ratio W/H were recorded. Some of the results are presented here, and in each figure, the experimentally determined aspect ratios are shown with the short vertical bars whose ends correspond to the possible minimum and maximum aspect ratios. In addition, theoretical calculations based on Equations (22) and (23) were carried out. The solid curve in each figure represents the model prediction and is calculated with some experimentally determined parameters. The horizontal line represents the aspect ratio of the completely relaxed drop. For the purpose of theoretical calculation, first the charge was calculated using Equation (19) followed by the apparent surface tension determination using Equation (20) for the fundamental mode and the capillary number from Equation (21). Subsequently, ω^* and δ^* were read off from Figs. 12 and 13 for the given Ca value to calculate the dimensioned values of ω and δ using Equation (24). The amplitudes A_1 and A_2 were established by the value of W/H at $t = 0$, together with the assumption that $d(W/H)/dt = 0$ at $t = 0$, which corresponds to the relaxation process starting from rest.

In Figs. 14-18, results are presented for the following cases (w-g refers to water-glycerin solution and Si-o refers to silicone-oil):

Fig.	Liquid type	a (mm)	η (mPa s)	Ca
14	Uncharged w-g	1.20	25	0.01
15	Uncharged Si-o	0.96	10	0.0045
16	Uncharged Si-o	1.1	100	0.446
17	Charged w-g	1.3	31	0.014
18	Charged Si-o	1.1	10	0.008

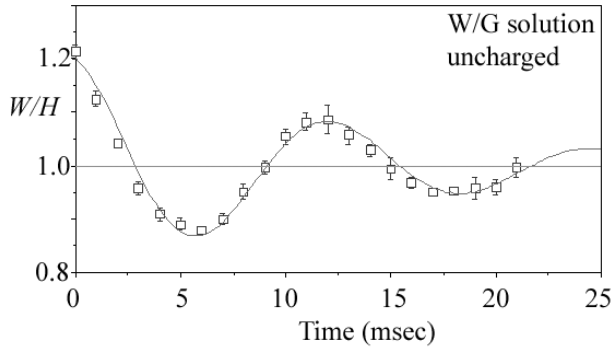

Fig. 14. Shape relaxation of an acoustically levitated uncharged W/G drop (a = 1.20 mm, Ca = 0.01) [6].

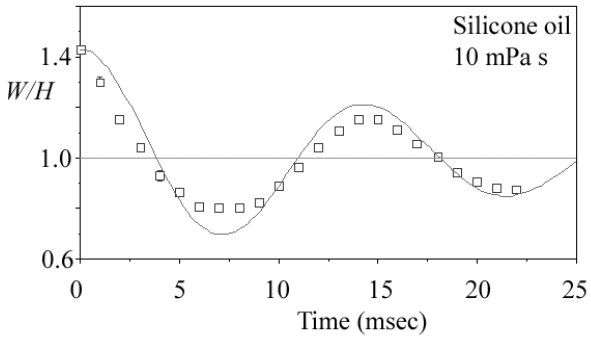

Fig. 15. Shape relaxation of an acoustically levitated silicone oil drop (a = 0.96 mm, Ca = 0.0045) [6].

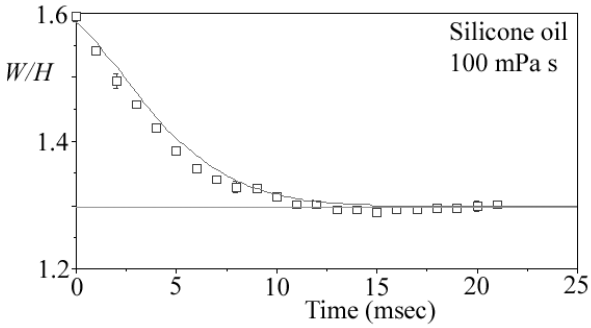

Fig. 16. Shape relaxation of an acoustically levitated silicone oil drop (a = 1.1 mm, Ca = 0.446) [6].

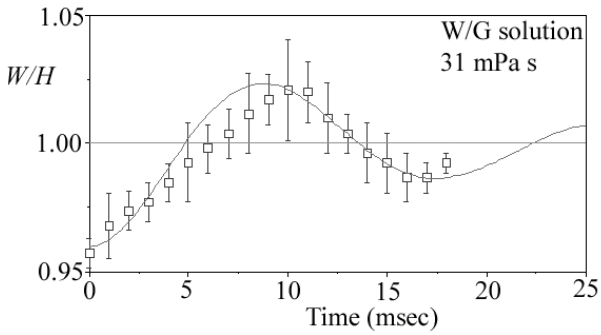

Fig. 17. Shape relaxation of an electrostatically levitated charged water-glycerin drop (a = 1.3 mm, Ca = 0.014) [6].

Fig. 14 for an uncharged water-glycerin solution drop shows good agreement with the theory. In Fig. 15, results for an acoustically levitated silicone-oil drop are presented. While the linear model appears to adequately the amplitude and the frequency of the relaxation process, some discrepancy in the apparent damping rate is seen. This may be attributed to the non-linearity in the system. Fig. 16 is the case of an overdamped uncharged silicone oil drop. Again, the agreement with theory is good, in spite of the large amplitude. The next two figures show results for electrostatically levitated drops. Fig. 17 shows the result for a charged water-glycerin solution drop. There is some discrepancy in the 5-10 ms range but remaining part of the relaxation process agrees well with the theory. Fig. 18 represents a result for a silicone oil drop. The damping is underpredicted to the extent that the error bars lie outside the theoretical curve. Since initial deformations are small, the nonlinear effects are unlikely to be the cause of this discrepancy. It is likely that the electrical conductivity plays a role in creating this discrepancy. Under electrostatic levitation, when the field is subsequently shut off, the charge undergoes redistribution. If the drop has non-zero conductivity, the redistribution is possibly not instantaneous. As a result, it is conceivable that the charge redistribution may contribute to the apparent stiffness.

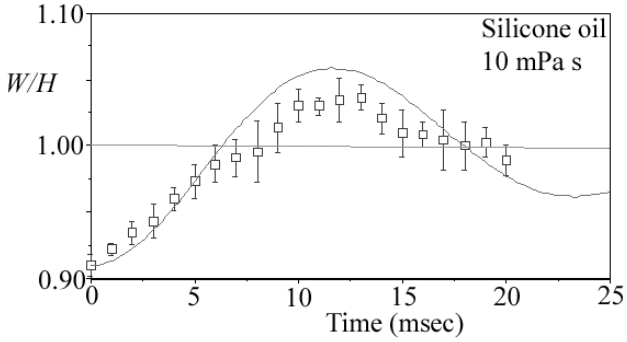

Fig. 18. Shape relaxation of an electrostatically levitated silicone-oil drop (a = 1.1 mm, Ca = 0.008) [6].

5. Thermal diffusivity measurement

Non-contact thermal diffusivity measurement of liquids is a bigger challenge than that for viscosity and surface tension because various phenomena such as buoyancy and thermocapillary flow set in when thermal stimuli are applied. While thermocapillary itself can be used as a measurement device (as discussed at the end of this section), buoyancy is particularly disruptive because it dominates over surface-driven fluid motion. Therefore, as a means to mitigate buoyancy-driven flow, acoustic-ally flattening of the drop into a horizontal disk has been applied, thereby reducing the gravitational potential [16]. For low-level thermal stimuli, thermocapillary flow may also be weak for the flat disk. Therefore, a pure conduction-based technique has been devised by Ohsaka, Redni-

kov & Sadhal [16]. The technique involved the acoustic levitation of a small amount of liquid in the shape of a drop and the application of a thermal stimulus with a CO_2 laser on the edge of the drop. Since the drop also rotates about the vertical axis, the heating is actually circumferential. The heated drop was then allowed to cool by heat loss from the surface (thermal relaxation). Due to acoustic streaming, the heat loss was quite non-uniform and appeared to occur mainly at the equator. While this approximation has been utilized [16], refined models can quite likely provide further improvement. The feasibility of the technique was demonstrated with the use of glycerin drops as a model liquid. This technique was also discussed in a previous review [27], and several of the details are repeated here for the sake of completeness and comparative analysis with a subsequent study [17].

5.1 Apparatus

The apparatus was the same as the one used for viscous damped oscillations (Fig. 10) but some modifications were made for the thermal measurements. A schematic exhibiting the experimental settings is shown in Fig. 19. As with the free-fall experiment, an ultrasonic transducer was used to generate a 23-kHz standing wave between the transducer head and the reflector, and liquid drop was levitated near a pressure node of the standing wave. Images of the levitated drop were captured by two video cameras located at the top and side of the levitator. These images were then used to determine the aspect ratio and actual dimensions of the drop. As mentioned earlier, a CO_2 laser aimed at the drop was used to heat the drop. The surface temperature of the drop was continuously monitored with an infrared (IR) camera looking down the drop.

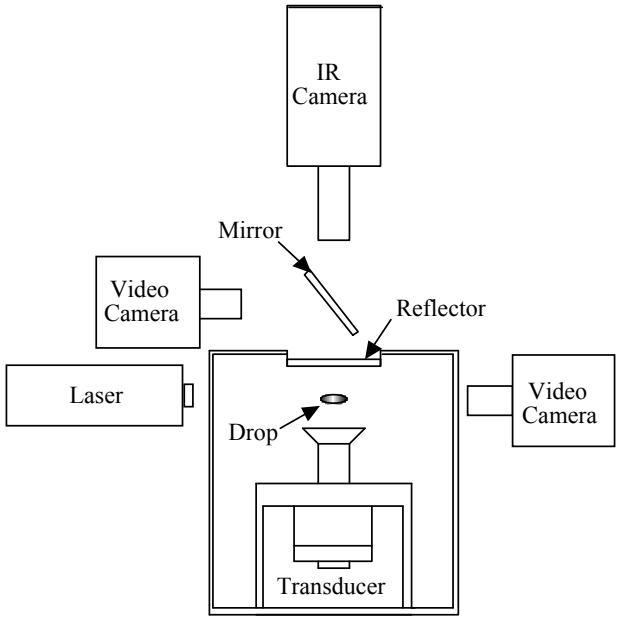

Fig. 19. Schematic of the experimental apparatus showing the key parts [16, 27]

5.2 Procedure

The procedure required the levitation of a small glycerin sample (approximately 15 μl) which was introduced into the levitation field with a hypodermic syringe. Upon detachment from the syringe, the sample and formed into an oblate spheroidal drop due to the action of various forces (gravity, surface tension and acoustic pressure), as shown in Fig. 20.

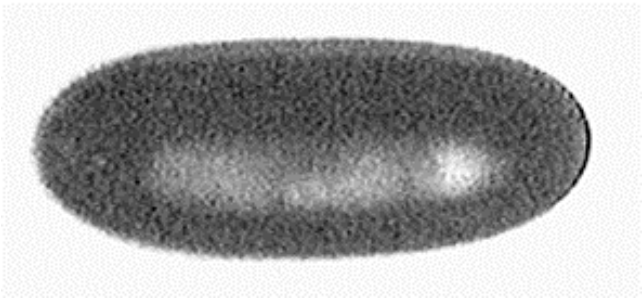

Fig. 20. Side view of an acoustically flattened drop with an aspect ratio of 2.6 [16, 27].

By varying the acoustic pressure, the drop aspect ratio, *a/b*, could be adjusted between 1.3 and 2.6. Here *a* and *b* are the equatorial and polar radii of the drop, respectively. The flattened drop shown in Fig. 20 has an aspect ratio of approximately 2.6. While maximum flattening would help mitigate buoyancy interference, further increasing the acoustic pressure would cause the top and bottom surfaces of the drop to dimple. Nevertheless, experiments and analysis with a dimpled drop have also been carried out, and are discussed in Section 5.4.

The CO_2 laser producing a narrow beam was turned on to locally heat the drop at a small area on the edge of the drop. The local heating caused the free-floating drop to rotate about the polar axis due to a thermally-driven torque. The result is a fairly uniform heating along the circumference. Conduction into the interior caused a rise in the drop temperature as a whole. After reaching a certain temperature, the laser was turned off and the drop is allowed to cool with the exterior convection.

A sequence of the IR images (0.5 s intervals) can be seen in Fig. 21, exhibiting the temperature at the top surface during the cooling process. Each color region represents a certain temperature range on the surface. The white circles superimposed on the first and last images indicate the circumference of the drop. To track the heat diffusion in time, a specific color ring is followed, and the prog-ression of that isotherm in time is recorded. The color being tracked is indicated by an arrow pointing to the ring in each image. As seen in this sequence of images, the selected isotherm gradually recedes and eventually disappears towards the centre. While the interior of the

drop continuously cools, the temperature at the circumference remains approximately constant at a temperature just above the ambient. Since the acoustic streaming pattern around the flattened drop is quite non-uniform, the convective heat loss from an acoustically levitated drop is also not uniform, and occurs mainly at the circumference. The receding rings are the result of internal heat flow toward the circumference.

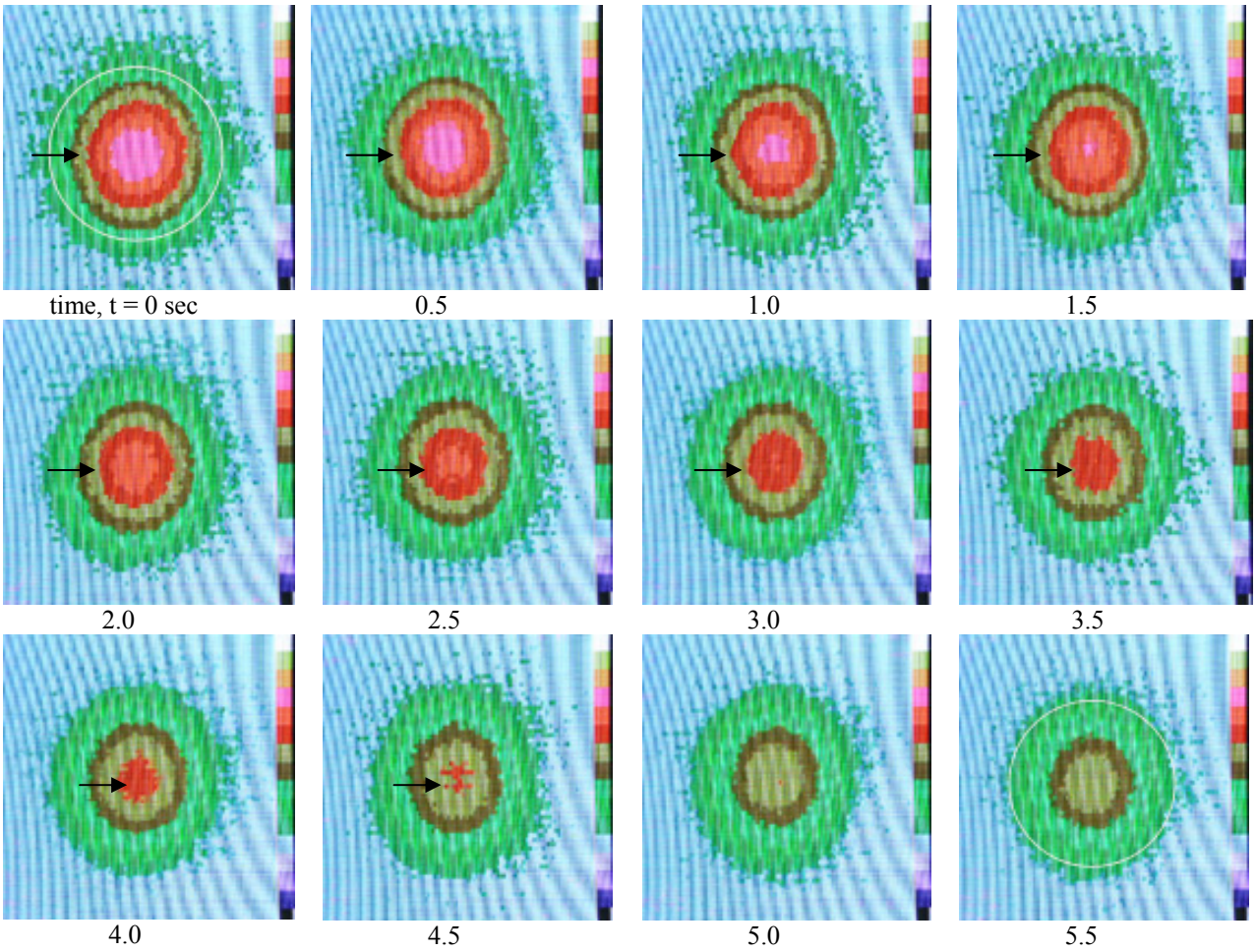

Fig. 21. A sequence of the IR images showing the receding thermal rings [16, 27].

5.3 Heat Flow Model

A simple one-dimensional radial flow heat conduction model was employed to establish a relationship between the selected isotherm and time. It was assumed that the heat loss at the circumference was predominant, and the temperature at the circumference was taken to remain constant at near a room temperature value. Under this approximation, no consideration was given to the heat loss from the top and bottom. The details of the governing equations are available in [16]. The numerical solution of the one-dimensional heat equation gave the time evolution of the temperature profile, and this allowed the location of the coordinates of a specific isotherm that represent a particular colour ring in the IR images. The calculations were performed using the known thermal diffusivity of glycerin together with comparisons with the experimental result.

5.4 Results and discussion

The position of the receding isotherm (show by arrows in Fig. 21) was measured and recorded. For the numerical calculation, the initial temperature distribution was determined from the first image. The property parameters were: drop spherical radius a = 0.26 cm, and thermal diffusivity α = 0.001 cm^2/sec. The plots of the isotherm tracking as a function of time from the experiment and the numerical calculation are given in Fig. 22. The experimental results show that the levitated glycerin drop has the apparent thermal diffusivity coefficient that is larger than the accepted value by 25%. The agreement between the experiment and the model turns out to be fair at best because of the highly simplified heat conduction model. One of the simplifications is lack of accounting of the heat loss from the top and bottom surfaces. In addition, the one-dimensional model does not take into consideration the

vertical temperature variation. Across-the-board correction for different materials may produce inconsistent results. For example, the 25% overprediction found for glycerin drops in the present measurement cannot be applied to water drops. Furthermore, the relationship between the aspect ratio and the sound pressure level varies for different materials. Therefore, the streaming intensity as well as the convective heat loss from the surface is material dependent. However, the technique is useful if it can be calibrated for various pressure levels and aspect ratios. The other alternative is to improve the analytical model. The convective transport with acoustic streaming has been modelled by Lee, Sadhal & Rednikov [17].

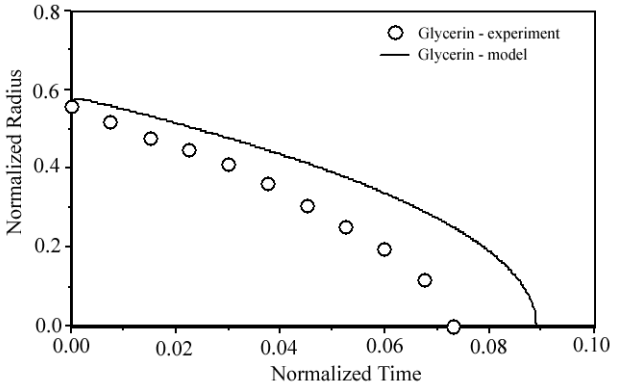

Fig. 22. The normalized radius of the receding ring representing a particular temperature as a function of the normalized time [16, 27].

Another technique using thermocapillary flow has been explored by Lee, Ohsaka, Rednikov & Sadhal [17]. The motivation was that the thermocapillary flow measurement and an analytical mode for this system could be used to solve the inverse problem. Here, the liquid disk was flattened to a thickness of 500μm and an aspect ratio of about 10. As mentioned before, the drop dimpled on the top and bottom surfaces. In addition, drop rotation was suppressed so that the thermal stimulation took place at a single spot, leading to asymmetric heating. Continuous heating at one spot produced sufficient intensity to set of thermocapillary flow. In addition, the intense acoustic field caused substantial surface heat loss besides the circumference so that this effect had to be properly accommodated. A theoretical model based on lubrication theory was set up for both fluid flow and heat transfer in the interior of the dimpled drop. The thermocapillary force term resulting from the surface tension on top and bottom boundaries became a part of the thickness-averaged momentum equation. It became necessary to consider dimpled drops (as opposed to flat ones) because otherwise, the thermocapillary-force term in this momentum equation became a conservative force leading to a trivial solution for the velocity field. The dimpled drop was assumed to have a concave paraboloidal shape profile both on the top and the bottom, and this was implemented into the lubrication approximation. In addition, the effect of acoustic streaming on heat transfer was modelled by using the flow field based on an oblate spheroid [28]. The transport mechanism with streaming is quite different from the usual convective transport. This different characterization arises particularly due to the slip velocity at the liquid-gas interface that is typical of acoustic streaming, as discussed in [18]. The dimensionless heat flux from the drop due to the exterior convection (Biot number) on the top surface (and identically the bottom) and side edge of glycerin drop were calculated from an acoustic streaming analysis.

The numerical analysis for the flattened drop involved an input of known viscosity values (as a function of temperature), constant but adjustable trial input values of the thermal diffusivity, laser heating rate, and Biot numbers (spatially varying) at the liquid-gas interfaces. Various thermal diffusivity inputs were used until good agreement of the thermal and the flow fields were obtained. The flow field was compared only qualitatively while for the thermal field, a more precise agreement is sought. A good agreement for the temperature distribution along the diameter of symmetry established the thermal diffusivity value. However, since the thermocapillary flow pattern and the temperature distribution measurements were largely qualitative, there was considerable error in the results which indicated no improvement over the thermal relaxation method. It may therefore be concluded that the thermal relaxation method would be better and investigators need to focus on improving on it, particularly the analytical part. With the analytical developments with the dimpled drop [17, 18], better analysis for the thermal relaxation method should not be very difficult.

6. Discussion

For understanding the basic thermodynamics of liquids in the undercooled region, it is important to measure the thermophysical properties of these materials. Since liquids in the undercooled state are sensitive to disruption by traditional measurement devices (e.g., probes), non-intrusive methods are necessary for the measurement. For this purpose, electrostatic and acoustic levitation of liquid samples are useful for achieving the undercooled state, as well as for the measurement. Resonant-frequency methods have been found to be effective for the non-contact measurement of viscosity and surface tension for low-viscosity liquids. For such cases, the surface oscillation frequency of the levitated samples is easily identifiable. Well-established theories correlate the surface tension to the frequency and the viscosity to the damping coefficient. For undercooled metallic melts in the viscosity range 1-130

mPa s, this technique has been successfully applied by Rhim *et al.* [4]. With increasing viscosity, as the damping gets more pronounced, the oscillations become more difficult to visualize. The shape of the sample (in the form of a liquid drop) is more sensitive to interference from external effects such as the gravity field and the levitation force. For such situations, in the medium viscosity range (0.1-100 Pa s), the shape-relaxation method under short-time free fall is an effective technique for determining the viscosity [6]. The free-fall, even though for a short time, significantly mitigates the gravitational effects and free relaxation with viscous damping is measurable. The investigators showed that the linear model based on the fundamental mode is adequate for acoustically levitated drops when the initial deformation is small. The discrepancies appeared in the drops with large initial deformations were attributed to nonlinear effects. Generally, the amplitude decay rates appeared higher than the linear model prediction. With electrostatic levitation, there is also an underprediction of damping, especially at the early stages of oscillation. It is possible that upon switching off the electric field, charge redistribution takes place and creates additional forces that bring about additional damping. For very viscous liquids with dynamic viscosity greater than 100 Pa s, the shape relaxation of a levitated drop, lobed by rotation proved to be sufficiently accurate.

The thermal diffusivity measurement techniques have left considerable room for improvement. The thermal relaxation method [6] relies on circumferential heating by a laser beam while the disk-shaped drop rotates. Upon cessation of heating, the reversal back towards isothermal conditions is allowed and the temperature distribution is thermographically recorded. On tracking a selected isotherm that propagates towards the center of the drop as it cools, and carrying this procedure out analytically as well, the inverse problem of thermal diffusivity is solved. The system being axisymmetric allows for a fairly simple analytical treatment. However, the modelling is perhaps too simple, and over-predicts the thermal diffusivity values when compared against known values. While the thermographic imaging seems quite accurate, the modelling needs more work, especially since the convective heat loss by acoustic streaming was approximated as an insulated boundary with heat loss occurring mainly on the edge. Also, with the aspect ratio being not very high, the one-dimensional approximation leaves possibilities for errors. Attempts with higher aspect ratio and focused spot-heating [16] together with an improved thermal transport model has not led to better accuracy of the thermal diffusivity measurement. The measurement technique relied on the thermocapillary flow visualization and thermographic imaging of the temperature distribution coupled with a lubrication-theory model for the flattened-disk drop. The technique utilized qualitative comparison between the theory and the experiment for the flow streamlines and the isotherm map. In view of the comparison being qualitative to solve the inverse problem, the results are prone to substantial error. It is felt that the thermal relaxation method with improved heat-transfer modelling would provide more accurate results for the thermal diffusivity.

References

[1] W. K. Rhim, K. Ohsaka, J. Cryst. Growth, **208**, 313 (2000).

[2] W. K. Rhim, K. Ohsaka, P.-F., Paradis, R. E. Spjut, Rev. Sci. Instrum., **70,** 2796 (1999).

[3] H. Lamb, Hydrodynamics, Cambridge University Press (1932).

[4] W. H. Reid, Q. Appl. Math. **18**, 86 (1960).

[5] K. Ohsaka, A. Rednikov, S.S. Sadhal, Trinh, E.H., Rev. Sci. Instrum., **73,** 2091 (2002).

[6] S. S. Sadhal, A. Rednikov, K. Ohsaka, Ann. New York Acad. Sci. **1027,** 447 (2004).

[7] S. Chandrasekhar, Proc. London Math. Soc. **9**(3), 141 (1959).

[8] S. Chandrasekhar, Hydrodynamic and Hydromagnetic Stability, Dover, New York (1961).

[9] C.A. Miller and L. E. Scriven, J. Fluid Mech. **32**, 417 (1968).

[10] A. Prosperetti, J. Mec. **19**, 149 (1980).

[11] P. L. Marston, J. Acoust. Soc. Am. 67, 15 (1980).

[12] E. Trinh, A. Zwern & T. G. Wang, J. Fluid Mech. **115**, 453 (1982).

[13] R.E. Apfel, Y. Tian, J. Jankovsky, T. Shi, X. Chen, R.G. Holt, E. Trinh, A. Croonquist, K.C. Thornton, A. Sacco, C. Coleman, F.W. Leslie, D.H. Matthiessen, Phys. Rev. Lett. **78**, 1912 (1997).

[14] K. Ohsaka, S. K. Chung, W. K. Rhim, Acta Mater. **46**, 4535 (1998).

[15] E.H. Trinh, P.L. Marston, J.L. Robey, J. Colloid Interface Sci. **124**, 95 (1988).

[16] K. Ohsaka, A. Rednikov, S.S. Sadhal, Ann. New York Acad. Sci., **974,** 124 (2002).

[17] S. Lee, S.S. Sadhal, & A.Y. Rednikov, Ann. New York Acad. Sci. **1077,** 75-95 (2006).

[18] S. Lee, S.S. Sadhal, A.Y. Rednikov, J. Heat Transfer **130,** 091602-1 (2008).

[19] J.W. S. Rayleigh, Phil. Mag. **14,** 184 (1882).

[20] J.Q. Feng, K.V. Beard, Proc. Roy. Soc. London, A**430,** 133 (1990)

[21] T. Iida, Z. Morita, J. Takeguchi, J. Jap. Inst. Met. **11,** 1169 (1975).

[22] M.G. Frohberg, M. Roesner-Kuhn, G.. Kuppermann, International Workshop on Nucleation and Thermophysical Properties of Undercooled Liquids, March 4-8, 1998, Physikzentrum Bad Honnef.

[23] S.-F. Chen, R.A. Overfelt, Int. J. Thermophysics **19,** 817 (1998).

[24] T. Ishikawa, P.-F. Paradis, T. Itami & S. Yoda, Measurement Sci. Tech. **16,** 443 (2005).
[25] T. Ishikawa, P.-F. Paradis N. Koike, Jpn. J. Appl. Phys. **45**, 1719 (2006).
[26] H. Mo, C. Zhou & W. Yu, J. Non-Newtonian Fluid Mech. **91,** 221 (2000).
[27] K. Ohsaka, A. Rednikov, S. S. Sadhal, Heat and Mass Transfer 2004, G. Vaidyanathan, B.V.S.S.S. Prasad, C. Balaji, Y. Joshi, Eds.,Proceedings of the Sixth ISHMT-ASME Heat and Mass Transfer Conference, January 5-7, 2004, Kalpakkam, India, pp 117-125, Tata McGraw-Hill. ISBN: 0-07-058350-1.
[28] A. Rednikov, S.S. Sadhal, J. Fluid Mech. **499,** 345 (2004).

*Corresponding author: sadhal@usc.edu